## Title
Flow-Induced Damage to Blood Cells in Aortic Valve Stenosis



## Journal
Annals of Biomedical Engineering, 44(9)

## ISSN
0145-3068

## Authors
Vahidkhah, Koohyar
Cordasco, Dan
Abbasi, Mostafa
et al.

## Publication Date
2016-09-01

## DOI
10.1007/s10439-016-1577-7

Peer reviewed

Published in final edited form as:
*Ann Biomed Eng*. 2016 September ; 44(9): 2724–2736. doi:10.1007/s10439-016-1577-7.

# Flow-Induced Damage to Blood Cells in Aortic Valve Stenosis

**KOOHYAR VAHIDKHAH**[1], **DAN CORDASCO**[2], **MOSTAFA ABBASI**[1], **LIANG GE**[3], **ELAINE TSENG**[3], **PROSENJIT BAGCHI**[2], **ALI N. AZADANI**[1]

[1]Cardiac Biomechanics Laboratory, Department of Mechanical and Materials Engineering, University of Denver, 2390 S. York St. #200, Denver, CO 80210, USA;

[2]Mechanical and Aerospace Engineering Department, Rutgers, The State University of New Jersey, Piscataway, NJ 08854, USA

[3]Department of Surgery, University of California at San Francisco Medical Center (UCSF), San Francisco, CA 94143-0118, USA

## Abstract

Valvular hemolysis and thrombosis are common complications associated with stenotic heart valves. This study aims to determine the extent to which hemodynamics induce such traumatic events. The viscous shear stress downstream of a severely calcified bioprosthetic valve was evaluated *via in vitro* 2D particle image velocimetry measurements. The blood cell membrane response to the measured stresses was then quantified using 3D immersed-boundary computational simulations. The shear stress level at the boundary layer of the jet flow formed downstream of the valve orifice was observed to reach a maximum of 1000–1700 dyn/cm$^2$, which was beyond the threshold values reported for platelet activation (100–1000 dyn/cm$^2$) and within the range of thresholds reported for red blood cell (RBC) damage (1000–2000 dyn/cm$^2$). Computational simulations demonstrated that the resultant tensions at the RBC membrane surface were unlikely to cause instant rupture, but likely to lead to membrane plastic failure. The resultant tensions at the platelet surface were also calculated and the potential damage was discussed. It was concluded that although shear-induced thrombotic trauma is very likely in stenotic heart valves, instant hemolysis is unlikely and the shear-induced damage to RBCs is mostly subhemolytic.

### Keywords

Valvular hemolysis and thrombosis; Flow-induced blood cell damage; Particle image velocimetry; 3D Immersed-boundary method

Address correspondence to Ali N. Azadani, Cardiac Biomechanics Laboratory, Department of Mechanical and Materials Engineering, University of Denver, 2390 S. York St. #200, Denver, CO 80210, USA. ali.azadani@du.eu.

ELECTRONIC SUPPLEMENTARY MATERIAL
The online version of this article (doi:10.1007/s10439-016-1577-7) contains supplementary material, which is available to authorized users.

CONFLICT OF INTEREST
The authors have no conflict of interest to declare.

## INTRODUCTION

Hemolysis and thrombosis are common complications of prosthetic aortic heart valves which result in significant morbidity and mortality. These conditions have also been reported in native aortic valve disease.[7,23,48] Contrary to prosthetic valves, where such complications may be initiated by bloodstream exposure to foreign surfaces, the predominant mechanism for platelet activation and red blood cell (RBC) damage in native stenotic valves may be mediated by high shear forces produced by the flow.[4,23] Stenotic valves often have a very small orifice, through which a strong jet flow emanates during systole. The jet velocity is typically much higher than the physiological blood flow through non-calcified aortic valves. The local increase in the flow velocity significantly increases the velocity gradient and in turn the shear stress level within the flow field. The extent to which hydrodynamic shearing forces could damage red blood cells and activate platelets is of great clinical importance, as it determines the potential need for preventive care such as anti-platelet/anti-coagulant treatment in patients with severe native aortic stenosis. It has been demonstrated that the true shear force experienced by individual blood cells is mainly determined by viscous rather than Reynolds shear stress (in the case of turbulence generation).[17,22] The elevated viscous shear stresses (SSs) experienced by blood cell membranes could result in traumatic events.

The SSs can be measured *in vitro via* particle image velocimetry (PIV), which has become a widely used technique in fluid dynamic assessment of prostheses in the past decades. The main advantage of this method compared to other techniques such as laser Doppler anemometry is the full-field velocity measurement of a selected plane with adequate spatial resolution. The majority of PIV investigations have been carried out in mechanical valves.[24] Lim *et al.*[27] were among the firsts to employ PIV to assess the flow dynamics of bioprosthetic valves. Although this technique has been applied to simulated calcified valves,[38,40] the flow field evaluation of an actual calcified bioprosthesis explanted from a patient as examined in this study has not been addressed yet.

The flow-induced blood cell damage is a multi-scale process in nature. Fluid viscous forces at the macroscale impart abnormal forces on the cell membrane at the microscale. In the case of RBCs, an increase in the resultant tensions beyond the membrane thresholds could cause immediate rupture (instant lysis), or permanent deformation and subsequently cell fragmentation.[11] Similarly, an increase in shear-induced deformation of the platelet membrane beyond a withstanding threshold could lead to morphological change and consequently activation.[25] More specifically, shear-induced reorganization and elongation of the cytoskeleton components,[28] as well as redistribution and clustering of receptor molecules on the platelet surface[18] promote platelet activation.

To examine the effects of hemodynamics on the blood cell membrane, computational simulation of the suspending cells deformation in shear flow, *via* fluid–solid interaction modeling, can be effectively employed. Detailed spatiotemporal variations of different important membrane parameters such as strain energy and principal tensions, which are experimentally difficult to capture, can be obtained by numerical modeling. Two major types of dynamics have been demonstrated for a freely suspended single RBC in a linear shear flow: tank-treading and tumbling. While the cell membrane and the interior

liquid make a continuous tank-treading-like rotation in the former (at high shear rates), a rigid body-like behavior resembling a flipping motion is observed in the latter (at low shear rates).[15,43] Similarly, the flipping motion of platelets in shear flows have been well established.[35] Computational simulations of blood cell dynamics *via* immersed-boundary methods in recent years have successfully reproduced these dynamics. They have further explored the effects of different parameters, e.g., cell deformability and cell–cell interaction, and subsequently discovered more complex behaviors like vacillating/breathing and swinging/tank-treading of RBCs, as well as the near-wall tumbling-to-sliding transition of platelets.[6,50,55] The focus of these studies has predominantly been the cell deformation and dynamics. Nevertheless, the computational models employed can be used to calculate the tensions at the cell surface[32] in order to analyze the potential for shear-induced traumatic phenomena.

This study aims to conduct an analysis of the flow-induced blood cell damage in stenotic aortic valves *via in vitro* measurements of the valve shearing force environment at the macroscale, and subsequently computer simulations of the corresponding mechanical response of the blood cell membrane at the microscale. As such, a comprehensive evaluation of the viscous shear stress downstream of a severely calcified bioprosthesis explanted from a patient is performed using high resolution 2D PIV measurements. The mechanical responses of an RBC and a platelet to the measured SSs are then determined by calculation of the resultant membrane tensions *via* high-fidelity 3D computational immersed-boundary simulations. Multiscale studies have recently emerged in the field of shear-induced blood cell damage.[13,14,34,54,56] Examples are the particle-based simulation of platelet morphological change during early shear-induced activation,[34] the particle dynamics simulation of hemolysis in mechanical heart valves,[13] the simulation of thrombogenesis *via* coupling a flow continuum model with a stochastic discrete cellular Potts model,[54] and the dissipative particle dynamics modeling of flow-induced RBC deformation.[14] The present study aims to complement such investigations by providing new insights on the mechanical force environment of stenotic heart valves and the resultant traumatic effects on blood cells by integrating macroscale *in vitro* measurements and microscale computational simulations.

## MATERIALS AND METHODS

### Experimental Setup

**Pulse Duplicator—**A degenerated 21 mm Carpentier-Edwards PERIMOUNT bioprosthesis explanted from a patient with severe aortic stenosis was obtained from Edwards Lifesciences, Inc. Calcification was present on all the leaflets with a very small tear, less than 0.5 mm, on one of the leaflets (Figs. 1a, 1b). The bioprosthesis was tested at room temperature in a custom-built pulse duplicator system (ViVitro Systems, Inc., Victoria, Canada). A schematic representation of the pulsatile flow model is shown in Fig. 1c. The valve is positioned axisymmetrically with respect to the flow measurements. Heart rate, blood pressure, and cardiac output were used as control parameters for the waveform generator controlling a servo pump. Input parameters matched ISO 5840 and FDA standards for testing heart valves: a heart rate of 70 beats/min, a 35% systolic duration of cycle period, mean atrial and aortic pressures of 10 and 100 mmHg, and a cardiac output of 5 L/min.

These parameters were maintained constant throughout the measurements. A recirculating glycerin solution in normal saline was used as the blood analog fluid. The fluid's refractive index was adjusted using sodium iodide to match that of the valve-mounting chamber and to minimize optical distortion. The approximate constituent concentration of the fluid was 79% sodium iodide, 20% glycerin, and 1% normal saline solution by volume.[5] The analog fluid at room temperature mimicked the blood viscosity at 37 °C (0.0035 Ns/$m^2$). Data acquisition was run over 10 consecutive cardiac cycles, and the transvalvular pressure gradient, regurgitant volume, and effective orifice area were determined. A detailed description of the flow loop is found in Azadani *et al.*[2]

**Particle Image Velocimetry—**A conventional 2D PIV system was used to obtain planar velocity measurements downstream of the bioprosthesis. Illumination was supplied by a dual oscillator Nd:YAG laser (New Wave Research SOLO II-30 Hz) and lasers were synchronized using a Laser Pulse Synchronizer (TSI, model 610034). Silver coated hollow glass particles (8 $\mu$m diameter, TSI, model 10089-SLVR) were used to visualize the flow. Images were recorded with a 1600 × 1200 pixel resolution cross-correlation CCD camera (Power View Plus 2MP, TSI, model 630057), capable of capturing PIV image pairs at 32 frames/s. A multi-grid PIV measurement was employed to capture shear stress magnitude within the jet boundary layer of the stenotic bioprosthesis (Fig. 1c). For grid-level 1, the camera was fitted to a NIKKOR lens (50 mm f/1.8D) and a narrow band interference filter was utilized to reduce reflections. To capture detailed flow structures of the viscous shear layer right above the bioprosthesis, extension rings were placed between the camera and the lens (grid-level 2). The spatial resolution for grid-levels 1 and 2 were 30.3 and 10.1 $\mu$m/pixel, respectively. Phase-locked measurements were acquired by triggering the PIV system from the pulse generator driving the piston pump, over 26 time instances regularly spaced over the entire cardiac cycle (860 ms). All images were correlated on a recursive Nyquist grid using a 50% overlap with a final pass interrogation window of 16 × 16 pixels. The final interrogation size was selected to have a careful balance between the highest resolution and the signal-to-noise ratio of the cross-correlations. Data were processed using INSIGHT 3G™ software. The principal viscous shear stress (termed as shear stress hereafter for simplicity) was calculated based on one-half of the difference between the largest and the smallest principal stresses.

## Computational Model

The computational model employed in this work was within the framework of the immersed-boundary method.[33] A detailed description of the method and its validation were presented in a prior publication.[8] Specifically, the validation of the RBC model against optical tweezer stretching experiments, and the validation of the flipping motion of platelets in simple shear flow against theory can be found in Cordasco and Bagchi,[6] and Vahidkhah *et al.*[50], respectively. The method consisted of three major modules: (i) the model for membrane deformation of a suspended blood cell, which was implemented using a finite element method (FEM). Within this module, the resultant forces due to the elastic deformation of the membrane were computed on a 3D triangular Lagrangian mesh that discretized the cell surface. (ii) The viscous fluid model which was implemented *via* a finite-difference projection-based CFD flow solver. This module computed the flow velocity

on an Eulerian grid taking into account the interpolated membrane forces. The projected flow velocities on the Lagrangian nodes were then used to compute the deformation of the cell. (iii) The two-way coupling between the flow dynamics and the membrane deformation which was implemented using the immersed-boundary method. This module interpolated the forces from the Lagrangian mesh to the Eulerian grid and the velocities from the fluid grid to the membrane mesh. The overall progression of the simulation method in a time step involves: (1) displacement of the Lagrangian nodes by the fluid flow through projection of fluid velocities onto the membrane nodes *via* interpolation, (2) computation of the deformation-induced elastic forces of the membrane mesh by FEM, (3) projection of those forces onto the flow grid *via* interpolation, and (4) eventually solution of the fluid domain under the effect of such forces. In what follows, the computational problem setup is presented and followed by a brief description of the above three modules.

**Problem Setup—**As schematically shown in Fig. 2, to evaluate the effect of the experimentally measured shearing forces on a blood cell, the cell was suspended in a linear shear flow between two parallel plates. The flow domain was a rectangular box that is periodic in $x$ and $z$ directions, $x$ being the flow direction, $y$ the direction of the velocity gradient, and z the vorticity direction. Here, $H = 27\ \mu$m, and $L = 18\ \mu$m. The no-slip condition was applied on the top and bottom plates. 181, 180, and 120 mesh points were employed in the $x$, $y$, and $z$ directions, respectively. The surface of the RBC and the platelet were discretized using 5120, and 1280 triangular elements, respectively. The independence of the numerical simulations from Eulerian/Lagrangian grid sizes, as well as the channel dimensions was verified separately (see supplementary material S1).

**Model for Blood Cells and the FEM—**The RBC was modeled as a liquid-filled elastic capsule of biconcave resting shape with an end-to-end distance of 7.8 $\mu$m.[16] The suspending medium (plasma) and the interior cytoplasm (rich in hemoglobin) were both assumed to be incompressible and Newtonian fluids with viscosities of 1.2 and 6.0 cP, respectively. The density of both liquids was assumed to be equal to that of water at 37 °C. The density difference between the interior/exterior fluids along with the gravity effects were neglected since our estimation of viscous vs. buoyancy forces on an RBC under high shear rates yielded significantly larger values (>5 orders of magnitude) for the viscous forces.

The model encompassed the essential properties of the RBC membrane, namely, resistance against shear deformation, area dilatation, and bending. The first two were modeled using the strain energy function developed by Skalak *et al.*[42]:

$$W_{\mathrm{e}} = \frac{G_{\mathrm{s}}}{2}\left(\frac{1}{2}I_1^2 + I_1 - I_2\right) + \frac{C}{8}I_2^2 \tag{1}$$

where $G_{\mathrm{s}}$ is the membrane shear elastic modulus, $C$ is the area dilatation constant, and $I_1$ and $I_2$ are the strain invariants of the Green strain tensor defined as $I_1 = \lambda_1^2 + \lambda_2^2 - 2$, and $I_1 = \lambda_1^2\lambda_2^2 - 1$, where $\lambda_1$ and $\lambda_2$ are the principal stretch ratios. $G_{\mathrm{s}}$ and $C$ were taken to be 0.005 and 200.0 dyn/cm, respectively.[12]

The principal elastic tensions per unit length were expressed as:[42]

$$T_1 = \frac{\lambda_1}{\lambda_2}\left[G_s\left(\lambda_1^2 - 1\right) + \frac{C}{2}\lambda_2^2 I_2\right]$$
$$T_2 = \frac{\lambda_2}{\lambda_1}\left[G_s\left(\lambda_2^2 - 1\right) + \frac{C}{2}\lambda_1^2 I_2\right] \quad (2)$$

and the maximum shear tension was computed from $\tau_{max} = \frac{1}{2}(T_2 - T_1)$. The cell membrane was discretized using flat triangular elements. In the FEM, the displacement, m, was assumed to vary linearly within each element, and was expressed in terms of linear shape functions, which were used to determine the deformation gradient tensor, and subsequently $\lambda_1$ and $\lambda_2$. The resultant elastic force at each node was then calculated by applying the principal of virtual work ($f_e = -\partial W_e/\partial v$). Helfrich's formulation[19] was used for the bending force density in the RBC membrane as $f_b = E_b\left[(2\kappa + c_0)\left(2\kappa^2 - 2\kappa_g - c_0\kappa\right) + 2\Delta_{LB}\kappa\right]n$, where $E_b$ is the bending modulus associated with the mean curvature $\kappa$, $c_0$ is the spontaneous curvature, $\kappa_g$ is the Gaussian curvature, $\Delta_{LB}$ is the Laplace–Beltrami operator, and $\boldsymbol{n}$ is the unit vector normal to the surface (see Yazdani and Bagchi[55] for details). The values of $E_b$ and $c_0$ were taken to be $7 \times 10^{-12}$ dyn.cm[10] and −2.09,[55] respectively.

The platelet was modeled as a nearly rigid oblate ellipsoid with an end-to-end distance of 3.6 $\mu$m and a thickness of 1.1 $\mu$m.[16] Skalak model (Eqs. (1)–(2)) was used with $G_s$ and $C$ increased by a factor of five compared to that of the RBC.[52] To reproduce the nearly rigid condition for the platelet membrane and to prevent its deformation under shearing forces, a bending model following Dupin *et al.*[9] with a very large bending stiffness constant was employed (see supplementary material S2).

**Flow Solver and Membrane Tracking—**The fluid motion at the cell length scale was modeled by the continuity and the Stokes equations, as the Reynolds number defined based on the equivalent radius of the RBC, $a_0 = (3V/4\pi)^{1/3}$ (V = 94.1 $\mu$m$^3$ being the RBC volume), was on the order $10^{-22}$. The computed membrane forces were added to the Stokes equations as body forces using the delta functions that vanish away from the cell membrane. The governing equations were solved in dimensionless form. $a_0$ was used as the length scale, and the inverse shear rate $\dot{\gamma}^{-1}$ as the time scale for non-dimensionalization. The dimensionless time was then denoted by $t^* = t\dot{\gamma}$. The cell membrane was advected by advecting the Lagrangian nodes as $dx/dt = u_m$, where $x$ was the node position, and the membrane velocity $u_m$ was obtained by interpolating the local fluid velocity using the delta function. The Stokes equations were solved on a fixed rectangular grid. The momentum equation was split into an advection–diffusion equation and a Poisson equation for the pressure. The body-force term was retained in the advection–diffusion equation. The nonlinear terms were treated explicitly using a second-order Adams–Bashforth scheme, and the viscous terms were treated semi-implicitly using the second-order Crank–Nicholson scheme. The resulting linear equations were inverted using an alternating direction implicit scheme to yield a predicted velocity field. The Poisson equation was then solved to obtain pressure at the next time level. Using the new pressure, the velocity field was corrected so that it satisfied the divergence-free condition.[8]

# RESULTS

## Flow Velocity Field and Shear Stress Environment Downstream of the Degenerated Bioprosthesis

Figure 3 shows the resulting physiological pressure and flow waveforms of the degenerated bioprosthesis.The mean pressure gradient was 61.2 ± 0.4 mmHg. The valvular effective orifice area and the regurgitation fraction were 0.67 $cm^2$ and 5.6%, respectively. The instantaneous velocity of the degenerated bioprosthesis based on grid level 1 is shown in Fig. 4a for the three main phases within the cardiac cycle namely, acceleration, peak flow, and deceleration. In the acceleration phase, a highly axial distribution of flow velocity along the bioprosthesis centerline is observed. The velocity components decreased abruptly from the strong central jet to the surrounding recirculating region. The flow profiles clearly showed decay of the jet as the flow moved downstream of the bioprosthesis due to viscous effects. Figure 4b shows the shear stress results of the grid level 2 measurement immediately downstream of the bioprosthesis. At the peak forward flow, a maximum velocity of 4.9 m/s occurred within the jet. The shear stress in the greater part of jet boundary layer was in the order of 100 Pa (1000 dyn/$cm^2$) and its magnitude was found to be consistent through different cardiac cycles. The shear stress levels within the jet and outside the jet boundary layer were much lower and on the order of 100 dyn/$cm^2$.

Figure 5 demonstrates the instantaneous shear stress profile 3 and 6 mm downstream of the bioprosthesis. It is observed that the peak shear stress (at the edge of the boundary layer) reaches values as high 1000 and 1700 dyn/$cm^2$, 6 and 3 mm downstream of the valve, respectively. It is also seen that inside the jet (less than 1 mm from the centerline of the jet) and outside of the jet (more than 1 mm from the shear layer), the shear stress is nearly 100 and 200 dyn/$cm^2$, respectively. In relatively closer proximity of the shear layer this value increases up to 300–500 dyn/$cm^2$.

## Blood Cell Deformation and the Resultant Cell Membrane Tensions

To investigate the potential detrimental effects of the measured SSs on the blood cell membrane, the computational flow setup described in Fig. 2 was employed at five different shear rates corresponding to SS = 100, 200, 300, 1000, and 1700 dyn/$cm^2$, based on the PIV results shown in Fig. 5. The following two sections present the results for an RBC and a platelet, respectively.

**RBC Flow Induced-Deformation—**Figure 6 demonstrates sample representative snapshots of the flow-induced deformation and elongation of an RBC under SS = 1700 dyn/$cm^2$. It was observed that the RBC began rotating due to the shearing torque until it reached a semi-steady orientation (3°–7° with respect to *x*-axis). Simultaneously, the shearing forces elongated the RBC until its biconcave resting shape was completely lost and transformed into an elongated prolate spheroid, similar to what was observed in previous experiments at similar shear rates.[46] Then, a semi-steady tank-treading behavior was observed. The elongation and the rotary motion of the cell membrane resulted in an increase in the membrane tensions. This was observed by the contours of the RBC membrane maximum shear tension, $\tau_{max}$ (force per unit length along 45° with respect to the principal axis

system orientation). Our results showed that the initial transience, during which the RBC significantly elongated and changed orientation with respect to the flow direction, was lost at around $t^* \sim 10$. Furthermore, our simulations with different initial RBC orientations have confirmed that this transience time, which is basically a characteristic time scale for RBC membrane response to shear, was nearly insensitive to the initial conditions. In the two cases of SS = 1000 and 1700 dyn/cm$^2$ this value corresponded to ~ 0.002 – 0.004s.

The objective of this study was to determine the effect of flow SS on the RBC membrane. Figure 7a demonstrates the temporal variations of the maximum value of $\tau_{max}$ or $\max(\tau_{max})$ at the RBC surface under different SSs. The minimum reported value for RBC membrane yield shear tension (0.02 dyn/cm) above which it exhibits permanent deformation is also shown in this figure.[11,51] It is seen that while $\max(\tau_{max})$ is below 0.02 dyn/cm for SS ≤ 300 dyn/cm$^2$, it oscillates between 0.025 and 0.08 dyn/cm for SS ≥ 1000 dyn/cm$^2$ and reaches values as high as 0.09 dyn/cm. It should be noted that the curves corresponding to SS = 1000 and 1700 dyn/cm$^2$ were not continued beyond $t^* \sim 80 – 90$ due to the fact that the semi-steady behavior was achieved and therefore computational efforts such as mesh smoothing methods to prevent mesh distortion under such pathological SSs was not justified. Figure 7b shows sample snapshots of the RBC membrane deformation and $\tau_{max}$ contours under different SSs when $\max(\tau_{max})$ is instantaneously maximum. It was observed that an increase in SS resulted in an increase in the RBC elongation and the corresponding magnitude of $\tau_{max}$. Our results for SS = 100–200 dyn/cm$^2$ showed values on the order of 0.01 dyn/cm for the principal tensions, $T_1$ and $T_2$, which is similar to the order of values calculated in a previous experimental work in the similar range of SS.[47] At SS = 1000–1700 dyn/cm$^2$, the principal tensions reached up to order of 0.1 dyn/cm.

Figure 7b further demonstrates that the RBC shapes under SS ≤ 300 dyn/cm$^2$ were significantly different than the ones under SS ≥1000 dyn/cm$^2$. This is because the RBC was undergoing different dynamics in the two different ranges of SS. At a higher SS the RBC exhibited a tank-treading motion, whereas at a lower SS the dynamics was a transitional behavior between tank-treading and tumbling (see supplementary material S3). Since the focus of this work was the magnitude of membrane resultant tensions, we did not delve into details of the RBC dynamics. There are a number of valuable computational works in this regard.[6,55]

**Platelet Flow-Induced Tension—**Figure 8 shows the results of our simulations for platelets. The regular periodic tumbling motion of the platelet due to shearing forces and the resultant membrane tensions are shown for the sample case of SS = 200 dyn/cm$^2$ in Fig. 8a. Figures 8b and 8c show the maximum values of $T_1$ and $\tau_{max}$ at the surface of a platelet under different SSs. $\max(T_1)$ was below 0.1 dyn/cm for SS = 100 dyn/cm$^2$ and between 0.2 and 1.5 dyn/cm for SS ≥ 200 dyn/cm$^2$, oscillating about 0.75–1.0 dyn/cm for SS ≥ 1000 dyn/cm$^2$. Also, while $\max(\tau_{max})$ lies below 0.003 dyn/cm for SS ≤ 300 dyn/cm$^2$ it reaches significantly larger values as high as 0.01–0.025 dyn/cm for SS ≥ 1000 dyn/cm$^2$. The reported value for platelet membrane rupture strength is also shown in Fig. 8b.[29] Figure 8d compares the contours of $\tau_{max}$ at the surface of a platelet under different SSs at $t^* \sim 30$.

Similar to the previous section, an increase in SS resulted in an increase in the magnitude of tensions.

## DISCUSSION

This study performed an analysis of shear-induced blood cell damage in stenotic heart valves. The shearing force environment induced by a severely stenotic bioprosthesis was quantified at the macroscale using PIV measurements; and the corresponding mechanical responses of the membrane of an RBC and a platelet were simulated using an immersed-boundary numerical method at the microscale. The results showed that the shear stress in the jet formed downstream of the stenotic valve reached values up to 1000–1700 dyn/cm$^2$. The simulations further demonstrated that the resultant principal tensions in the RBC and platelet membranes under such high SSs reached values on the orders of 0.1 and 1.0 dyn/cm, respectively. The corresponding membrane maximum shear tension was observed to be in the range of 0.025–0.09 dyn/cm for an RBC and 0.005–0.025 dyn/cm for a platelet.

RBC hemolytic trauma and platelet activation are both known to not only depend on the cell contact with foreign surfaces, but also on the flow shear stress magnitude. Flow-induced blood damage has been studied in different flow systems, e.g., concentric cylinder and cone-and-plate viscometers, parallel plate flow chambers, and jet flows injected into RBC suspensions.[44] In these studies, the extent to which the contact with foreign surfaces affect trauma to blood cells remained unclear. The shear-induced threshold for RBC hemolysis and platelet activation measured in these studies both span a wide range from levels of $10^3$ to $10^4$ dyn/cm$^2$, and from $10^2$ to $10^3$ dyn/cm$^2$, respectively.[44] The results of these studies can be unified by the concept of exposure time: the higher it gets, the lower the stress threshold level for cell damage.[20,26] Table 1 shows examples of the reported threshold ranges and the corresponding exposure times. Note that threshold values as high as 40,000 dyn/cm$^2$ have also been reported for RBC damage at exposure times on the order of $10^{-5}$ s.[44] On the other hand, it has been observed that platelets that had been briefly pre-exposed to high SSs are activated under physiological low SSs if the exposure time reaches the level of $10^3$ s.[41] Regardless of which mechanism is dominant, foreign surfaces or in-bulk shear, an increase in the exposure time increases the damage to blood cells due to increased cell dispersion in the former, and the viscoplastic time-dependent response of the cell membrane (after the membrane tensions exceeds the yield shear) in the latter.[44] In this perspective, significantly large values of shear-stress threshold corresponding to very small exposure times are attributed to the instantaneous tensile failure of the RBC membrane.[45]

The results of our PIV measurements demonstrated that the shear stress levels at the viscous layer were beyond the platelet activation threshold, and within the range of thresholds reported for RBC hemolysis. The estimation of a blood cell's residence time in the shear layer (where highest SSs would be exerted on its membrane) from our PIV results *via* tracking imaginary massless particles gave a value on the order of $10^{-2}$–$10^{-1}$ s. Comparing these two values with the data presented in Table 1 indicates that although a thrombotic complication is very likely to take place due to the stenotic valve, the occurrence of RBC hemolytic trauma is unclear. It should be noted that since this study aims to isolate the potential biophysical effects of fluid flow on thrombogenesis, the biochemical processes

which trigger the platelet activation such as release of thrombin and ADP are not taken into account and the shear-induced morphological alterations are focused as platelet activation.

Our computational simulations elucidated the extent to which shear induces damage on a blood cell. The distribution of principal tensions at the RBC surface demonstrated that the occurrence of instant hemolysis was unlikely as the calculated values—on the order of (0.01–0.1 dyn/cm)—were two orders of magnitude smaller than the values reported in the literature for tensile rupture of the RBC membrane, which is 10–20 dyn/cm.[11,12] While the instant membrane rupture in the jet shear layer was unlikely, the viscoplastic breakdown of the RBC membrane was expected to occur as the maximum shear tension obtained from our simulations exceeded the yield shear for plastic failure of the membrane, which is 0.02–0.08 dyn/cm.[11,51] It should be noted that since the residence time of a blood cell in the shear layer (0.01–0.1 s) was one order of magnitude larger than the characteristic time scale for RBC response to shear (0.002–0.004 s), the RBCs flowing inside the shear layer would indeed experience such large values of $\tau_{max}$. Another important notion here is how the residence time compares to the characteristic time for viscoplastic response of the RBC membrane $t_0 = 2\eta_p/\tau_0$, where $\eta_p$ is the viscosity of plastic flow of the RBC membrane and $\tau_0$ is its yield shear.[11] Taking $\tau_0 = 0.02 – 0.08$ dyn/cm[11] and $\eta_p = 0.001 – 0.002$ dyn s/cm at 37 °C[51] gives a range of $t_0 = 0.025 – 0.2$ s. Since this range was similar to the estimated cell residence time range, it was inferred that the permanent deformation of the RBC membrane due to plastic failure is likely. Previous experimental studies have also demonstrated that shearing forces which do not produce hemolysis may lead to permanent subhemolytic alterations in the RBC membrane biophysical/biochemical properties, which in turn results in a decreased rate of RBC survival[30,31,46] (an illustrative example is the clearing of misshapen RBCs in spleen[39]), and consequently morbidities such as anemia.

Unlike the case of RBCs where plenty of experimental data are found regarding the membrane strength, experimental works providing similar data for platelets are limited. McGrath *et al.*[29] reported a value of 0.2 dyn/cm for the platelet membrane rupture strength. Our results showed that the tension created in the platelet membrane exceeded this value when SS ≥ 200 dyn/cm$^2$, which could be an indication of platelet lysis. It should also be noted that the range at which platelet lysis takes place is reported as SS = 100–600 dyn/cm[21,21] Although it has been suggested the shear-induced resultant tensions in the platelet membrane could lead to activation,[25,56] a threshold for membrane tensions above which such phenomena occurs does not exist in the literature. Hence, further analysis of our results is only possible when more quantitative experimental data on the relationship between platelet activation and membrane tensions is acquired.

One of the limitations of the present study was using 2D PIV measurements which neglect the third velocity component. However, since the axial jet velocity is of such great magnitude, the third velocity component is negligible. Another limitation was neglecting the effects of RBC–RBC interactions on their response to the shearing environment. A previous experiment[26] has demonstrated the insensitivity of hemolytic trauma to blood hematocrit and hence the RBC–RBC interaction. On the other hand, a recent computational study[32] on pairwise interaction of RBCs in simple shear flow has shown significant effects of cell–cell interaction on their membrane tension. Hence, many-cell simulations are required to

determine the effects of the simplification employed in the present work. The heterogeneous cellular interactions (RBC-platelet) were neglected considering the significantly lower number density of platelets compared to RBCs, as well as the notion that the effect of an RBC on a platelet is mainly laterally displacing it in the shear flow rather than generating deformation-induced tension in its membrane.[49] It should also be noted that we examined the cell response under laminar flow conditions. This assumption was reasonable as the jet flow regime close to the valve orifice, which was of our greatest interest, was indeed laminar. In addition, previous studies have shown the insignificance of turbulence effects at the cell length scale.[44–46] It is also important to note that our computational model does not include the inertial terms as the Reynolds number defined based on the cell size lies on the order of 0.01 for the lower SSs considered. However, at the highest SSs under consideration it increased up to the order of 0.1, the effect of which could become important. It is also known that the membrane of RBC/platelet is negatively charged, which affects the cell–cell interactions. Considering the fact that the focus of the present study was the hydrodynamic effects, such property was not taken into account.

This study is unique in the sense that it attempts to connect the experimental data on blood cell membrane yield shear and rupture strength, to the flow-induced blood cell damage in stenotic heart valves by employing a multiscale approach that integrates macroscale experimental measurement and microscale computational simulation. The results of the present study have demonstrated a significant likelihood of platelet activation leading to thrombotic trauma as well as subhemolytic permanent damage to RBCs due to stenotic heart valves.

## Supplementary Material

Refer to Web version on PubMed Central for supplementary material.

## ACKNOWLEDGMENTS

This work was supported by the American Heart Association and University of Denver Postdoctoral Fellowship Award. We thank Bruce Van Daman from Edwards Lifesciences for providing us with the degenerated PERIMOUNT bioprosthesis. Computational support from SOE HPC at Rutgers University, School of Engineering is acknowledged.

## REFERENCES

1. Anderson GH, Hellums JD, Moake JL, and Alfrey CP Jr. Platelet lysis and aggregation in shear fields. Blood Cells 4:499–511, 1978. [PubMed: 162570]
2. Azadani AN, Jaussaud N, Matthews PB, Ge L, Chuter TAM, and Tseng EE Transcatheter aortic valves inadequately relieve stenosis in small degenerated bioprostheses. Interact. CardioVasc. Thorac. Surg 11:70–77, 2010. [PubMed: 20395249]
3. Bacher RP, and Williams MC Hemolysis in capillary flow. J. Lab. Clin. Med 76:485, 1970. [PubMed: 4917796]
4. Becker RC, Eisenberg P, and Turpie AGG Pathobiologic features and prevention of thrombotic complications associated with prosthetic heart valves: fundamental principles and the contribution of platelets and thrombin. Am. Heart J 141:1025–1037, 2001. [PubMed: 11376320]
5. Browne P, Ramuzat A, Saxena R, and Yoganathan AP Experimental investigation of the steady flow downstream of the St. Jude bileaflet heart valve: a comparison between laser Doppler

velocimetry and particle image velocimetry techniques. Ann. Biomed. Eng 28:39–47, 2000. [PubMed: 10645786]

6. Cordasco D, and Bagchi P. Intermittency and synchronized motion of red blood cell dynamics in shear flow. J. Fluid Mech 759:472–488, 2014.
7. Dimitrow PP, Hlawaty M, Undas A, Sniezek-Maciejewska M, Sobien B, Stepien E, and Tracz W. Effect of aortic valve stenosis on haemostasis is independent from vascular atherosclerotic burden. Atherosclerosis 204:103–108, 2009.
8. Doddi SK, and Bagchi P. Three-dimensional computational modeling of multiple deformable cells flowing in microvessels. Phys. Rev. E 79:046318, 2009.
9. Dupin MM, Halliday I, Care CM, Alboul L, and Munn LL Modeling the flow of dense suspensions of deformable particles in three dimensions. Phys. Rev. E 75:066707, 2007.
10. Evans EA Bending elastic-modulus of red-blood-cell membrane derived from buckling instability in micropipet aspiration tests. Biophys. J 43:27–30, 1983. [PubMed: 6882860]
11. Evans EA, and Hochmuth RM Membrane viscoplastic flow. Biophys. J 16:13–26, 1976. [PubMed: 1244887]
12. Evans EA, Waugh R, and Melnik L. Elastic area compressibility modulus of red-cell membrane. Biophys. J 16:585–595, 1976. [PubMed: 1276386]
13. Ezzeldin HM, de Tullio MD, Vanella M, Solares SD, and Balaras E. A strain-based model for mechanical hemolysis based on a coarse-grained red blood cell model. Ann. Biomed. Eng 43:1398–1409, 2015. [PubMed: 25691396]
14. Fedosov DA, Lei H, Caswell B, Suresh S, and Karniadakis GE Multiscale modeling of red blood cell mechanics and blood flow in malaria. PLoS Comput. Biol 7:e1002270, 2011.
15. Fischer TM, Stohrliesen M, and Schmidschonbein H. Red-cell as a fluid droplet—tank tread-like motion of human erythrocyte-membrane in shear-flow. Science 202:894–896, 1978. [PubMed: 715448]
16. Fung YC Biomechanics: Mechanical Properties of Living Tissues. New York: Springer, 1993.
17. Ge L, Dasi LP, Sotiropoulos F, and Yoganathan AP Characterization of hemodynamic forces induced by mechanical heart valves: Reynolds vs. viscous stresses. Ann. Biomed. Eng 36:276–297, 2008. [PubMed: 18049902]
18. Gitz E, Koopman CD, Giannas A, Koekman CA, van den Heuvel DJ, Deckmyn H, Akkerman JW, Gerritsen HC, and Urbanus RT Platelet interaction with von Willebrand factor is enhanced by shear-induced clustering of glycoprotein Ibalpha. Haematologica 98:1810–1818, 2013. [PubMed: 23753027]
19. Helfrich W. Elastic properties of lipid bilayers—theory and possible experiments. Zeitschrift Fur Naturforschung C-J. Biosci. C 28:693–703, 1973.
20. Hellums JD 1993 Whitaker lecture—biorheology in thrombosis research. Ann. Biomed. Eng 22:445–455, 1994. [PubMed: 7825747]
21. Hung TC, Hochmuth RM, Joist JH, and Sutera SP Shear-induced aggregation and lysis of platelets. Trans. Am. Soc. Artif. Intern. Organs 22:285–291, 1976. [PubMed: 821202]
22. Jones SA A relationship between reynolds stresses and viscous dissipation—implications to red-cell damage. Ann. Biomed. Eng 23:21–28, 1995. [PubMed: 7762879]
23. Kawase I, Matsuo T, Sasayama K, Suzuki H, and Nishikawa H. Hemolytic anemia with aortic stenosis resolved by urgent aortic valve replacement. Ann. Thorac. Surg 86:645–646, 2008. [PubMed: 18640351]
24. Kheradvar A, Groves EM, Falahatpisheh A, Mofrad MK, Alavi SH, Tranquillo R, Dasi LP, Simmons CA, Grande-Allen KJ, Goergen CJ, Baaijens F, Little SH, Canic S, and Griffith B. Emerging trends in heart valve engineering: Part IV. Computational modeling and experimental studies. Ann. Biomed. Eng 43:2314–2333, 2015. [PubMed: 26224522]
25. Leung SL LY, Bluestein D, Slepian MJ. Dielectrophoresis-mediated electrodeformation as a means of determining individual platelet stiffness. Ann. Biomed. Eng 2015.
26. Leverett LB, Lynch EC, Alfrey CP, and Hellums JD Red blood-cell damage by shear-stress. Biophys. J 12:257, 1972. [PubMed: 5016112]

27. Lim WL, Chew YT, Chew TC, and Low HT Pulsatile flow studies of a porcine bioprosthetic aortic valve *in vitro*: PIV measurements and shear-induced blood damage. J. Biomech 34:1417–1427, 2001. [PubMed: 11672716]
28. Maxwell MJ, Dopheide SM, Turner SJ, and Jackson SP Shear induces a unique series of morphological changes in translocating platelets—effects of morphology on translocation dynamics. Arterioscler. Thromb. Vasc. Biol 26:663–669, 2006. [PubMed: 16385083]
29. McGrath B, Mealing G, and Labrosse MR A mechanobiological investigation of platelets. Biomech. Model. Mechanobiol 10:473–484, 2011. [PubMed: 20706764]
30. Nanjappa BN, Chang HK, and Glomski CA Trauma of the erythrocyte membrane associated with low shear stress. Biophys. J 13:1212–1222, 1973. [PubMed: 4754200]
31. Ohta Y, Okamoto H, Kanno M, and Okuda T. Atomic force microscopic observation of mechanically traumatized erythrocytes. Artif. Organs 26:10–17, 2002. [PubMed: 11872006]
32. Omori T, Ishikawa T, Imai Y, and Yamaguchi T. Membrane tension of red blood cells pairwisely interacting in simple shear flow. J. Biomech 46:548–553, 2013. [PubMed: 23102822]
33. Peskin CS, and Mcqueen DM Modeling prosthetic heart-valves for numerical-analysis of blood-flow in the heart. J. Comput. Phys 37:113–132, 1980.
34. Pothapragada S, Zhang P, Sheriff J, Livelli M, Slepian MJ, Deng YF and Bluestein D. A phenomenological particle-based platelet model for simulating filopodia formation during early activation. International J. Numer. Methods Biomed. Eng 31: 2015.
35. Pozrikidis C. Flipping of an adherent blood platelet over a substrate. J. Fluid Mech 568:161–172, 2006.
36. Ramstack JM, Zuckerman L, and Mockros LF Shear-induced activation of platelets. J. Biomech 12:113–125, 1979. [PubMed: 422576]
37. Rooney JA Hemolysis near an ultrasonically pulsating gas bubble. Science 169:869–871, 1970. [PubMed: 5432582]
38. Saikrishnan N, Yap CH, Milligan NC, Vasilyev NV, and Yoganathan AP *In vitro* characterization of bicuspid aortic valve hemodynamics using particle image velocimetry. Ann. Biomed. Eng 40:1760–1775, 2012. [PubMed: 22318396]
39. Sandza JG, Clark RE, Weldon CS, and Sutera SP Subhemolytic trauma of erythrocytes: recognition and sequestration by the spleen as a function of shear. Trans. Am. Soc. Artif. Intern. Organs 20:457–462, 1974. [PubMed: 4615410]
40. Seaman C, Akingba AG, and Sucosky P. Steady flow hemodynamic and energy loss measurements in normal and simulated calcified tricuspid and bicuspid aortic valves. J. Biomech. Eng.-Trans. ASME 136:041001, 2014.
41. Sheriff J, Bluestein D, Girdhar G, and Jesty J. High-shear stress sensitizes platelets to subsequent low-shear conditions. Ann. Biomed. Eng 38:1442–1450, 2010. [PubMed: 20135353]
42. Skalak R, Tozeren A, Zarda RP, and Chien S. Strain energy function of red blood-cell membranes. Biophys. J 13:245–280, 1973. [PubMed: 4697236]
43. Skotheim JM, and Secomb TW Red blood cells and other nonspherical capsules in shear flow: oscillatory dynamics and the tank-treading-to-tumbling transition. Phys. Rev. Lett 98:078301, 2007.
44. Sutera SP Flow-induced trauma to blood-cells. Circ. Res 41:2–8, 1977. [PubMed: 324656]
45. Sutera SP, Croce PA, and Mehrjard M. Hemolysis and subhemolytic alterations of human RBC induced by turbulent shear-flow. Trans. Am. Soc. Artif. Intern. Organs 18:335–341, 1972. [PubMed: 4679885]
46. Sutera SP, and Mehrjardi MH Deformation and fragmentation of human red blood-cells in turbulent shear-flow. Biophys. J 15:1–10, 1975. [PubMed: 1174639]
47. Transontay R, Sutera SP, Zahalak GI, and Rao PR Membrane stress and internal-pressure in a red-blood-cell freely suspended in a shear-flow. Biophys. J 51:915–924, 1987. [PubMed: 3607212]
48. Tsuji A, Tanabe M, Onishi K, Kitamura T, Okinaka T, Ito M, Isaka N, and Nakano T. Intravascular hemolysis in aortic stenosis. Intern. Med 43:935–938, 2004. [PubMed: 15575243]

Health Research Alliance Author Manuscript


49. Vahidkhah K, Diamond SL, and Bagchi P. Hydrodynamic interaction between a platelet and an erythrocyte: effect of erythrocyte deformability, dynamics, and wall proximity. J. Biomech. Eng 135:51002, 2013. [PubMed: 24231958]
50. Vahidkhah K, Diamond SL, and Bagchi P. Platelet dynamics in three-dimensional simulation of whole blood. Biophys. J 106:2529–2540, 2014. [PubMed: 24896133]
51. Waugh RE Temperature dependence of the yield shear resultant and the plastic viscosity coefficient of erythrocyte membrane. Implications about molecular events during membrane failure. Biophys. J 39:273–278, 1982. [PubMed: 7139026]
52. White JG, Burris SM, Tukey D, Smith C, and Clawson CC Micropipette aspiration of human-platelets—influence of microtubules and actin-filaments on deformability. Blood 64:210–214, 1984. [PubMed: 6145458]
53. Williams AR Release of serotonin from human platelets by acoustic microstreaming. J. Acoust. Soc. Am 56:1640–1649, 1974. [PubMed: 4427036]
54. Xu ZL, Lioi J, Mu J, Kamocka MM, Liu XM, Chen DZ, Rosen ED, and Alber M. A multiscale model of venous thrombus formation with surface-mediated control of blood coagulation cascade. Biophys. J 98:1723–1732, 2010. [PubMed: 20441735]
55. Yazdani AZK, and Bagchi P. Phase diagram and breathing dynamics of a single red blood cell and a biconcave capsule in dilute shear flow. Phys. Rev. E 84:026314, 2011.
56. Zhang P, Gao C, Zhang N, Slepian MJ, Deng YF, and Bluestein D. Multiscale particle-based modeling of flowing platelets in blood plasma using dissipative particle dynamics and coarse grained molecular dynamics. Cell. Mol. Bioeng 7:552–574, 2014. [PubMed: 25530818]

Health Research Alliance Author Manuscript

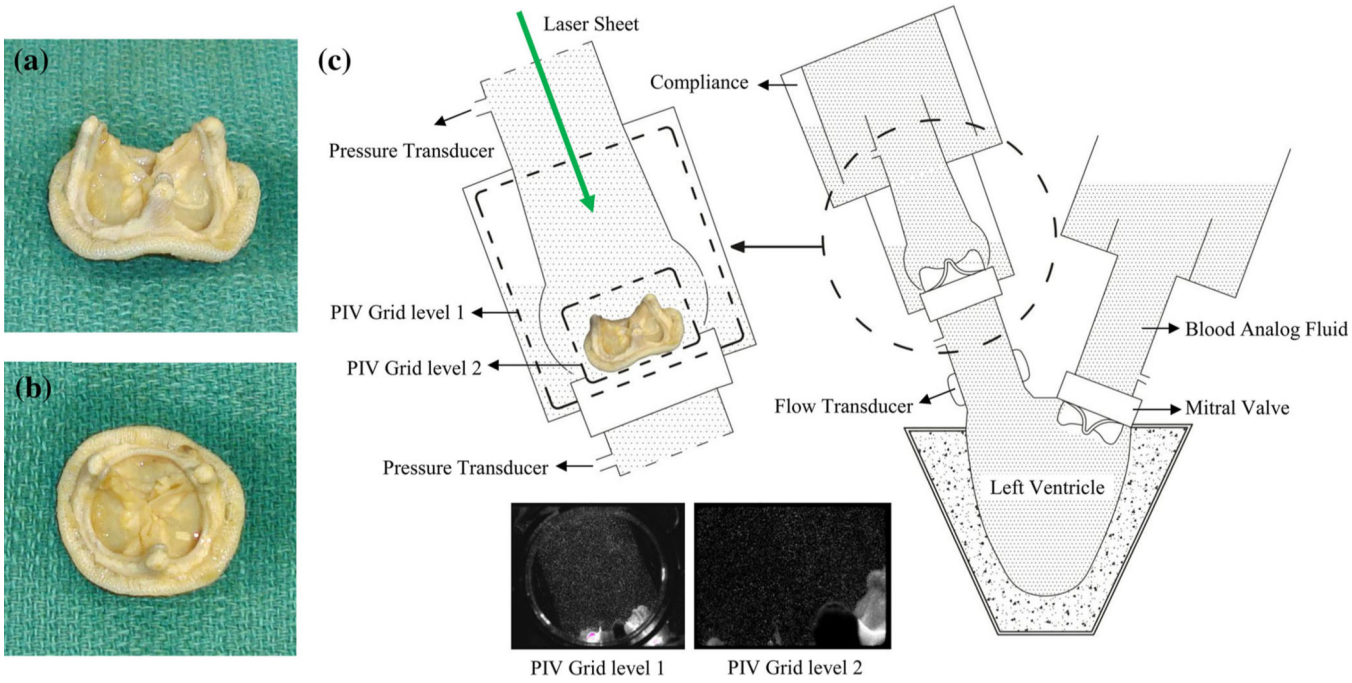


**FIGURE 1.**

(a) Side and (b) top views of the degenerated aortic bioprosthesis. (c) Schematic of the pulse duplicator and PIV grid levels.

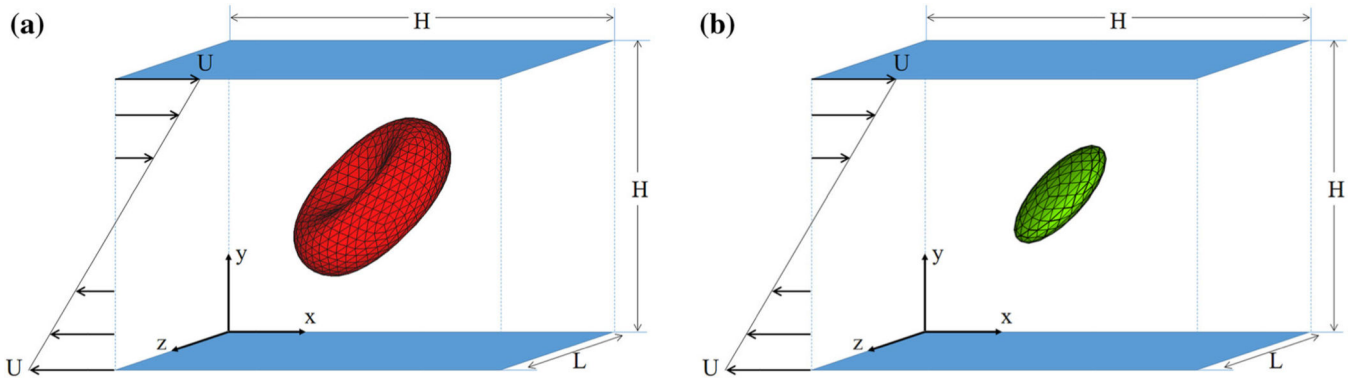


**FIGURE 2.**

Schematic of the computational setup for a red blood cell (a) and a platelet (b). The actual number of triangles in the Lagrangian mesh is higher than what is shown.

Health Research Alliance Author Manuscript

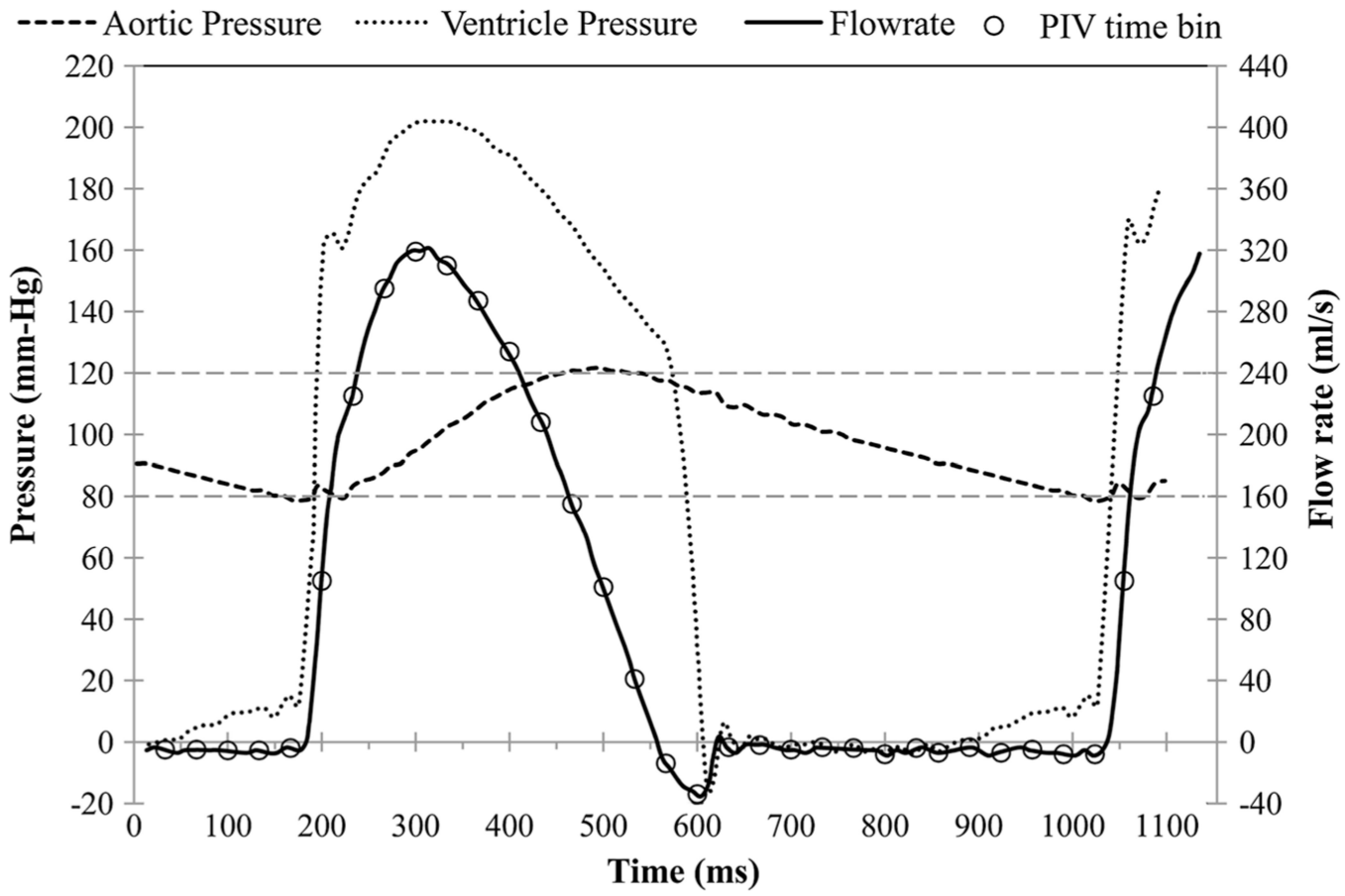


**FIGURE 3.**
Bioprosthetic pressure and flow rate waveforms.

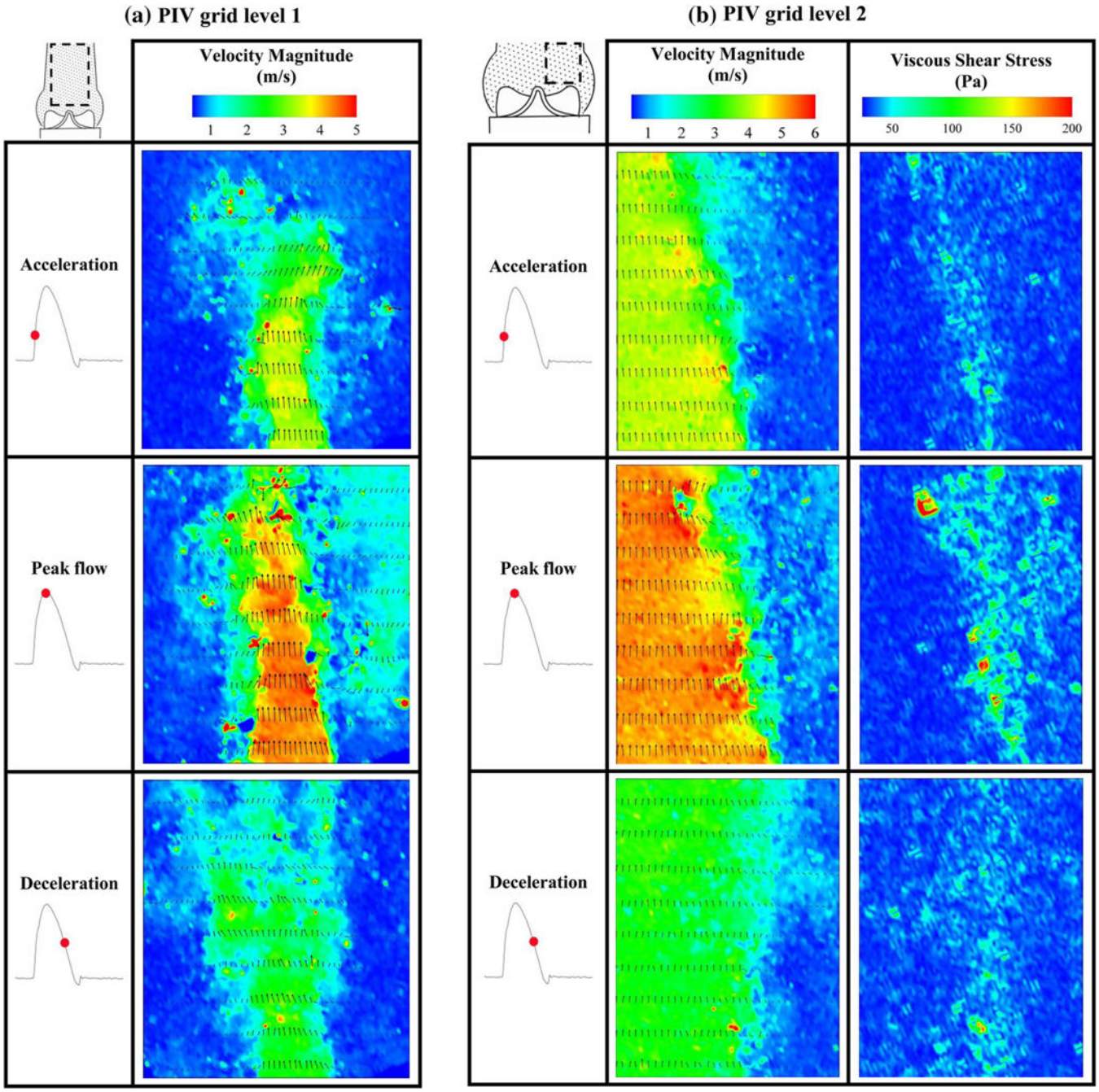


**FIGURE 4.**

Instantaneous velocity and shear stress fields obtained from grid level 1 (a) and grid level 2 (b) PIV measurements.

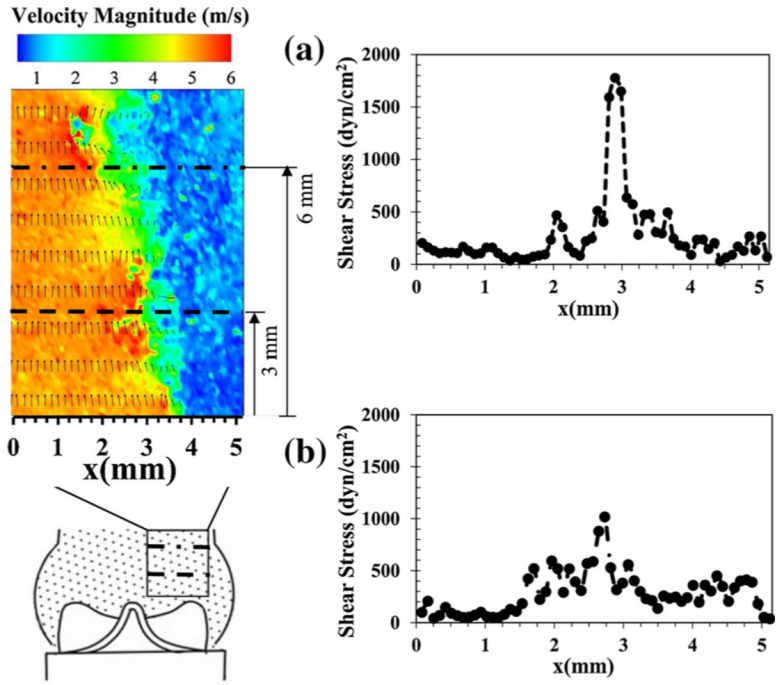


**FIGURE 5.**

Instantaneous shear profile 3 mm (a) shown by dashed line, and 6 mm (b) shown by dash-dotted line, downstream of the bioprosthesis at the peak flow. A velocity contour plot at the peak flow is presented on the left side.

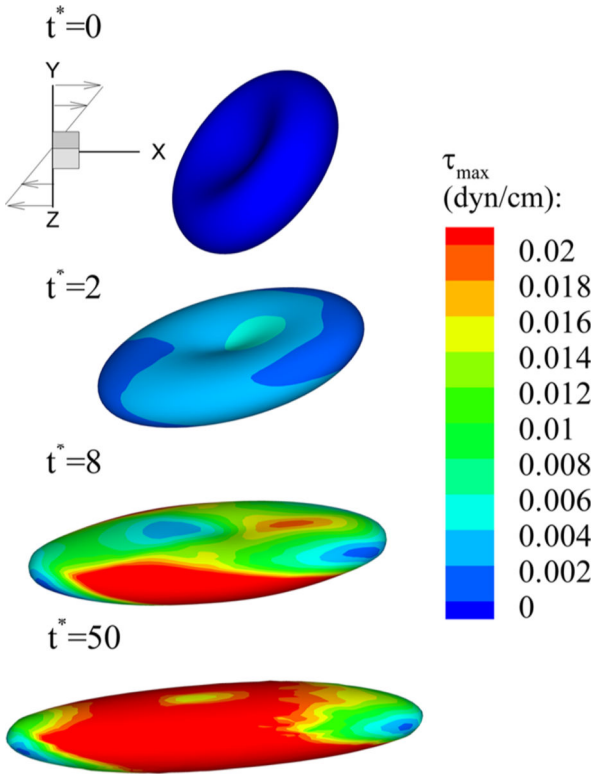


**FIGURE 6.**

Representative snapshots of the deformation of an RBC under SS = 1700 dyn/cm$^2$. Contours of maximum shear tension are also shown. The dimensionless time is $t^* = t\dot{\gamma}$, $\dot{\gamma}$ being the shear rate.

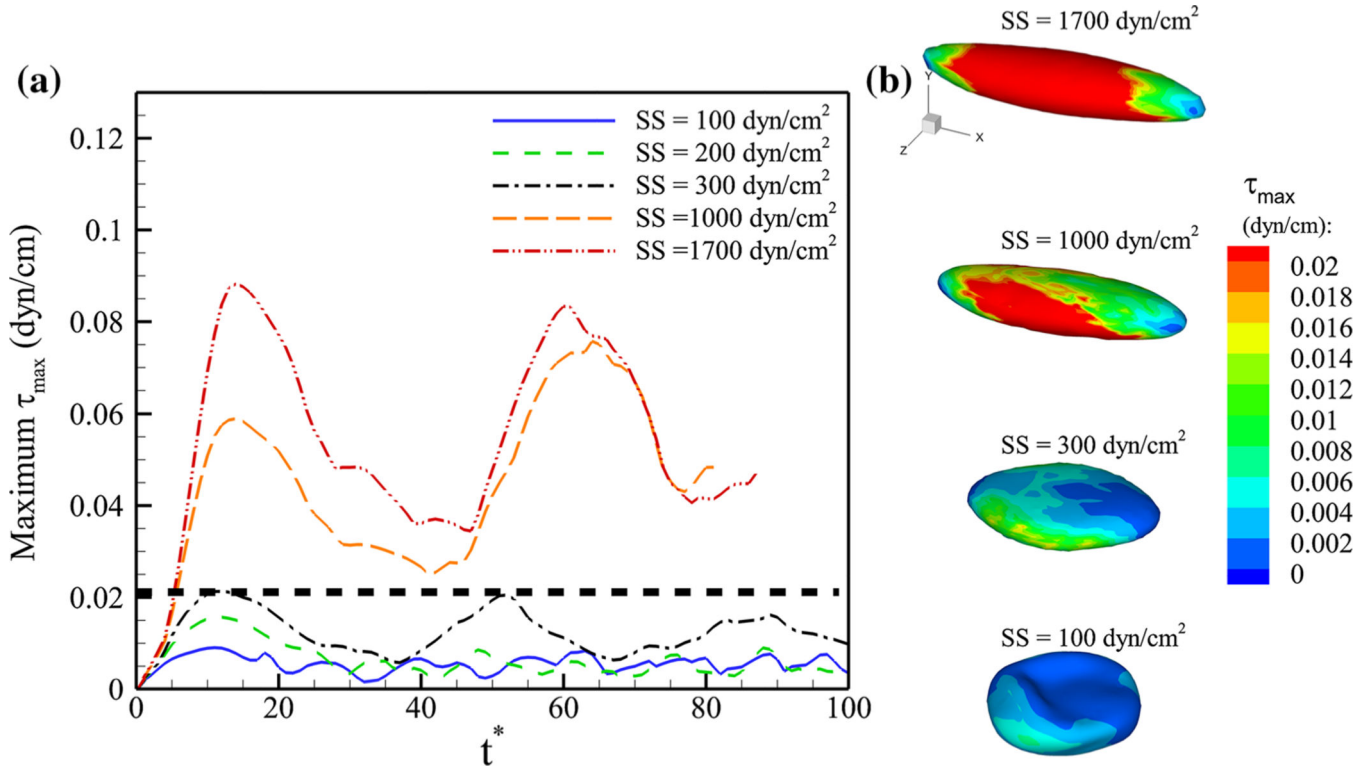


**FIGURE 7.**

(a) Temporal variations in max($\tau_{max}$) at the surface of an RBC membrane under different SSs. The straight dashed line shows the RBC membrane yield shear reported in the literature[11,51]. (b) Contours of $\tau_{max}$ at the surface of an RBC membrane under different SSs when max($\tau_{max}$) is instantaneously maximum ($t^*$ ~ 60 for SS = 1700 and 1000 dyn/cm$^2$, $t^*$ ~ 50 for SS = 300 dyn/cm$^2$, and $t^*$ ~ 40 for SS = 100 dyn/cm$^2$).

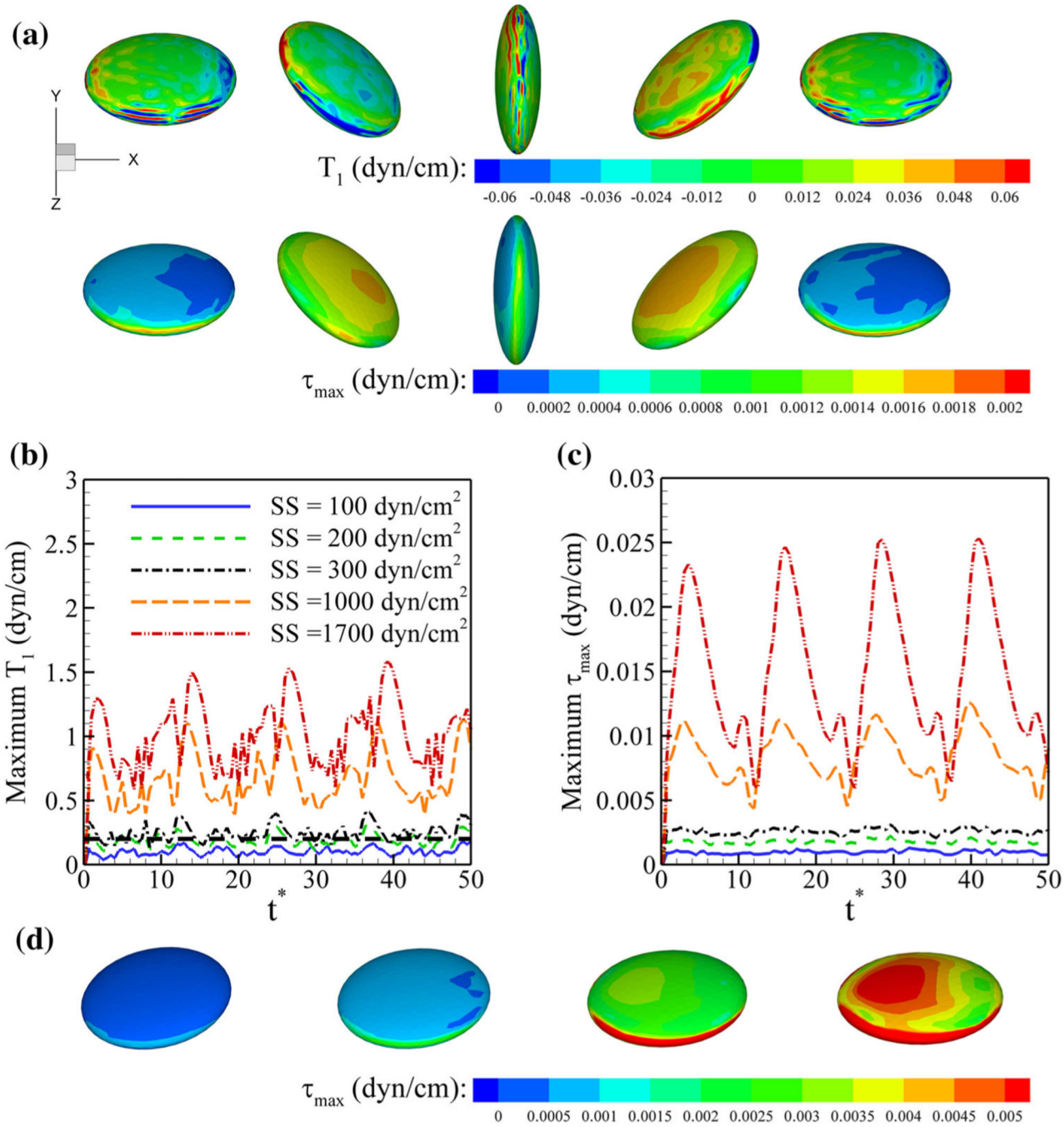


**FIGURE 8.**

(a) Representative snapshots of the tumbling motion of a platelet under SS = 200 dyn/cm$^2$. $t^*$ = 5.0, 9.8, 11.3, 12.6, and 17.3 from left to right. Contours of $T_1$ ((a)—top row) and $\tau_{max}$ ((a)—bottom row) at the platelet surface are also shown. Temporal variations in max($T_1$) (b) and max($\tau_{max}$) (c) at the surface of a platelet under different shear stresses. The straight dashed line in (b) shows the platelet membrane rupture strength reported in the literature[29].

(d) Distribution of $\tau_{max}$ at the platelet surface at $t^* \sim 30$ under SS = 100, 300, 1000, and 1700 dyn/cm$^2$ from left to right.



Health Research Alliance Author Manuscript

**TABLE 1.**

Shear stress threshold range and the corresponding exposure times for shear-induced blood cell damage.

| Shear stress threshold range (dyn/cm$^2$) | Order of exposure time (s) | Reference |
|---|---|---|
| Red blood cell | | |
| 500–1000 | $10^3$ | Sutera *et al.*[45] |
| 1500 | $10^2$ | Leverett *et al.*[26] |
| 2500 | $10^2$ | Sutera and Mehrjardi [46] |
| 5000 | $10^{-2}$ | Bacher and Williams [3] |
| 4500 | $10^{-3}$ | Rooney *et al.*[37] |
| Platelet | | |
| 100–165 | $10^2$ | Hung *et al.*[21] |
| 130 | $10^{-3}$ | Williams [53] |
| 300–1000 | $10^{-2}$–$10^1$ | Ramstack *et al.*[36] |